Received: 4 February 2018 | Revised: 5 October 2018 | Accepted: 20 October 2018

DOI: 10.1002/stc.2288

RESEARCH ARTICLE

WILEY

Damage detection in structural systems utilizing artificial neural networks and proper orthogonal decomposition

Saeed Eftekhar Azam | Ahmed Rageh | Daniel Linzell

Department of Civil Engineering, University of Nebraska–Lincoln, Lincoln, Nebraska, United States

Correspondence
Saeed Eftekhar Azam, Department of Civil Engineering, University of Nebraska–Lincoln, 2200 Vine St, Lincoln, NE 68503.
Email: eftekhar-azam@unl.edu

Funding information
Spokes: MEDIUM: MIDWEST: Smart Big Data Pipeline for Aging Rural Bridge Transportation Infrastructure, Grant/Award Number: 1762034

Summary

A supervised learning scheme is proposed for detecting, locating, and quantifying the intensity of damage in structures using Artificial Neural Networks (ANNs) and Proper Orthogonal Decomposition (POD). For structural systems, such as buildings and bridges, Proper Orthogonal Modes (POMs) associated with their response are functions of (1) applied external loads and (2) mechanistic properties. In the present research, a supervised learning strategy was adopted to help discriminate POM variations because of damage from damage caused by applied load variations. A neural classifier was trained to categorize response to different load patterns, and a regression ANN was subsequently trained using an ensemble of applied loads to detect possible damage from the categorized POMs. To demonstrate the effectiveness of the proposed approach, simulated experiments were performed with the intent of identifying damage indices for a railway truss bridge. A validated, three-dimensional (3D) finite element (FE) model of an existing bridge was used to generate strain time histories under train loads measured from weigh-in-motion (WIM) stations near the bridge. The efficacy of the proposed method was demonstrated through these simulated experiments.

KEYWORDS

artificial neural network, classification, damage detection, proper orthogonal decomposition, regression, strain

1 | INTRODUCTION

Aging infrastructure, the increased popularity of performance-based design and the demand for rapid verification of newly proposed design concepts necessitate accurate monitoring of infrastructure health. In the context of transportation infrastructure, namely, bridges, current monitoring practice is based on visual inspections at prescribed frequencies, a process that is subject to human error and, in the limit, may fail to reveal significant damage in a timely manner.[1] Additionally, performing visual inspections at prescribed frequencies, oftentimes approaching 24 months, regardless of the state of health of the structure could be inefficient.[2] These concerns have motivated extensive research on smart monitoring of structural condition. In this context, the process of implementing a continuous and autonomous damage identification scheme for civil structures is commonly referred to as structural health monitoring (SHM). This work has shown that structural deficiencies oftentimes cannot be measured directly.[3] Therefore, detection methods focus on extracting damage features that are "hidden" in recorded sensor data. One of the major, recent research

objectives in the SHM community has been development of automated feature extraction algorithms that enable autonomous damage identification methods when structures are subjected to various demands.

In many cases, a structural deficiency is caused by degradation of material properties or changes in its geometry and, therefore, variations in the structure's dynamic properties. It is known that modal properties such as curvature,[4,5] eigenmodes,[6-8] and modal strain energy[9,10] are sensitive to these types of deficiencies. The most common approach for vibration-based damage detection is executed in two stages: modal identification and model updating. An optimization procedure is employed to find the set of parameters that minimize an objective function that represents user-defined discrepancy norms between damage features extracted from measured response and corresponding damage features from a predictive model. A major challenge associated with application of identified modal properties for damage detection under operational conditions is that variations in environmental conditions, such as temperature and wind speed, increase uncertainties and may drastically affect modal identification results. Variations in modal properties from environmental conditions often overshadow changes from structural deficiencies. To separate these inputs, Moaveni et al. adopted a static polynomial model to represent relationships between identified natural frequencies and measured temperatures.[11] Hu et al. conducted a comparative study between different statistical approaches for removing environmental and/or operational effects using a large, continuously collected dynamic response data set from a pedestrian bridge.[12] Additionally, most operational modal analysis (OMA) algorithms equate ambient excitations to stationary, white noise. In many cases such assumptions might be violated, and consequently, modal properties would not be identified in a consistent manner. Research to address issues caused by nonstationary external inputs is in progress.[13,14]

In addition to uncertainties stemming from modal identification, modeling errors also affect damage estimates. Moaveni et al. performed shake table tests of a full scale, seven story reinforced concrete building to study uncertainties in common damage detection methods.[15] Uncertainty and sensitivity analyses associated with damage detection using modal identification and finite element (FE) model updating were completed. It was concluded that the level of confidence in damage identification results is a function of level of uncertainty in identified modal parameters; choices made during design of the experiments (e.g., spatial density of measurements); and modeling errors (e.g., mesh size).[6,16] To provide a systematic analysis and damage identification scheme, Papadimitriou et al. adopted transitional Markov chain Monte Carlo for Bayesian damage identification.[17] Recently, Bayesian-based OMA damage identification has gained attention in the research community.[18-20] To alleviate the effects of OMA uncertainties, a number of studies have focused on model updating using time domain signals. Erazo et al. proposed an offline method based on an unscented Kalman filter and Markov chain Monte Carlo for system and input identification.[21] Astroza et al. proposed a joint input parameter estimation for nonlinear, distributed plasticity systems.[22] Performance of the aforementioned methods relies profoundly on the number of unknown parameters in the system,[23] model class selection,[24] and user expertise.

The aforementioned issues associated with OMA, parameter identification, and stochasticity of excitation sources have motivated SHM research focused on statistical response analysis. They include inaccuracies associated with automatic damage feature extraction under operational conditions; the “curse of dimensionality” when dealing with relatively large parameter sets; addressing unknown and nonstationary external excitations, a particular problem for in-service bridges; and previous failures associated with pinpointing local damage using conventional damage detection methods. These items have focused on identifying deviations from normal structural conditions using statistical analyses of sensor data.[25] O'Connor et al. implemented a continuous monitoring system on a highway bridge and used coupled Statistical Process Control (SPC) and Gaussian Process Regression (GPR) for centralized damage identification based on novelty detection.[26] GPR was employed to eliminate statistical variations caused by vehicle–bridge interaction and environmental effects, and relatively long duration time series were used to determine the SPC threshold. Dervilis et al. performed laboratory fatigue tests of a wind turbine blade and adopted Machine Learning methods, including various Neural Networks, to detect damage based on changes in sensor data principal components.[27] Ou et al. completed a similar study on a prototype wind turbine and compared SHM schemes based on statistical damage features with those based on modal parameters. It was concluded that statistically based methods outperformed modal-based methods and succeeded in identifying induced damage, even at low-damage levels.[28] Although these statistical novelty detection methods have been proven to be effective for damage identification, the training period to address statistical variability caused by thermal fluctuations can take several months or even years.[26,29] Farrar and Worden[3] state that one of the axioms of SHM is that damage presence and severity can be identified in a supervised learning mode. Another SHM axiom asserts that for system damage assessment, a comparison between two system states is required. It can subsequently be deduced that identification of the type and severity of structural damage can either be accomplished using

a comprehensive set of experiments on the healthy structure or by using an accurate numerical model of the system. In practice, the former requirement is not feasible, and accurate numerical models are needed.

A vibration-based, damage detection framework with damage features assumed to have linear or weakly nonlinear dependence to variations in ambient temperature[30] is proposed by the authors. This approach could potentially reduce required training periods for the algorithm and provide damage features using relatively simple computational techniques. To this end, variations in Proper Orthogonal Modes (POMs) from an array of sensors were adopted as damage features. POMs are directly extracted from structural response and are theoretically sensitive to both changes in system parameters and in external excitation. A number of experimental and numerical studies have been performed to investigate POM sensitivity to various damage scenarios. Ruotolo et al. completed one of the first investigations of Proper Orthogonal Decomposition (POD)-based damage detection.[31] They proposed a damage index based on singular frequency response function values from structure accelerations and successfully detected stiffness reductions in a truss member under different operational conditions. Vanlanduit et al. proposed using robust singular-value decomposition (SVD) to detect damage from changes in velocity spectra subspaces when the damaged structure was subjected to different nonstructural surface treatments.[32] Galvanetto et al. have performed a similar study but adopted variations in Proper Orthogonal Values (POVs) as damage indices.[33] More recently, Shane et al. employed POD to detect damage severity and location in a composite beam numerical model.[34] Eftekhar Azam et al. studied damage detection in a building subjected to base shear excitations using variations in an SVD subspace.[23,35] Bellino et al. proposed a PCA-based method for detecting damage in linear time-varying systems.[36] Lanata et al. developed a method for static damage detection in beams via simulated experiments using POD.[37] Xia et al. completed an investigation of damage detection using principal component analysis (PCA) of dynamic strain data from a simulated bridge.[38] To date, all damage detection efforts utilizing POD-based feature extraction have focused on either broadband or stationary structure excitations. Those assumptions are often violated in real-life situations. To evaluate the effects of nonstationarity input on POD-based reduced-order models subject to various seismic excitations, Eftekhar Azam et al. trained a POD subspace of structural response of the Pirelli Tower in Milan subjected to El Centro earthquake time histories and verified the accuracy of the trained model when Kobe and Friuli time histories were used to excite the structure.[39]

Artificial neural networks (ANNs) furnish a generic, nonlinear parameterized mapping between an ensemble of inputs and a set of outputs. Once an ANN is trained on available sample data, it can recognize patterns; therefore, ANNs are suitable tools for signature analysis.[40] During the past few decades, ANNs have been widely studied in association with damage identification in structural systems. Recently, Jin et al. used an extended Kalman filter for estimating weights of a regression neural network for damage detection of a highway bridge under severe temperature changes.[41] Dworakowski et al. proposed a classification neural network for fatigue damage detection in aircraft.[42] Gu et al. proposed a framework based on ANN for removing false positive SHM alarms stemming from temperature variations.[43] Sbarufatti proposed a framework for optimizing ANN hyperparameters based on analysis of variance and used the optimized ANN for fatigue damage identification.[44] Various ANN architectures have been proposed with feed-forward architecture being the most commonly used in several applications, including health monitoring of mechanical and structural systems,[45] because of simplicity and versatility. For a literature survey on applications of ANN to structural health monitoring, readers are referred to Amezquita-Sanchez and Adeli.[45]

A framework is presented, herein, to detect damage under operational conditions using coupled POD and ANNs. In doing so, it is assumed that during the structure's operational life, there are no measurements of system input. When dealing with structures, system input is most often the external loads. For the current study, these are train axle loads and, given that those loads are not measured, this can be classified as an output-only damage detection method. A supervised learning scheme is proposed for output-only classification of structural response that reduces POM variations belonging to each defined class of structural response. An ANN-based regression analysis was performed to quantify relationships between identified POMs and damage severity and location. A simulated experiment, in which a set of field-measured train loads were applied to FE models of an existing, double track, railroad, truss bridge, was designed to demonstrate the efficacy of the proposed method. To train the ANNs, noisy, simulated strain time histories at damage-prone locations were used to obtain POMs of the structure under different damage scenarios. Discrete, nonstationary loading scenarios, such as those from a train traversing the bridge, were used as inputs. Because of the relatively short duration of each loading event, it was assumed that environmental variabilities are negligible within the time interval of each train passage. However, for different time intervals or under different loading conditions, it is understood that environmental variability may need to be included. This topic is the focus of a follow-up study.

2 | FEATURE EXTRACTION USING POD

POD autonomously searches sensor measurements for interdependencies between data that is normally assumed to act independently. This is accomplished through calculating a set of ordered and orthonormal basis vectors based on the portion of energy that each basis vector could capture.[46] This approach has been applied to numerous fields, including statistics, computational fluid dynamics, and image processing. When applied to systems of finite dimension, it is referred to as Principal Component Analysis (PCA) and its origins are found in work by Pearson on fitting planes and lines to point sets.[47] When applied to distributed parameter systems, it is called Karhunen–Loève decomposition (KLD).[48] Single Value Decomposition (SVD) was proposed as extension of eigenvalue decomposition of general, nonsquare matrices.[49] Liang et al. provided a detailed discussion of similarities and differences between PCA, KLD, and SVD.[50]

A central problem in neural network research is finding an appropriate representation of multivariate data, with independent component analysis (ICA) and PCA being two commonly applied feature extraction methods.[51] ICA is used to find components that are maximally independent and non-Gaussian and has been widely used for structural dynamics OMA of lightly damped structures subject to broadband ambient excitations.[52] Recently, Yang et al. have studied its application to OMA of heavily damped structures.[53] Ghahari et al. performed an investigation of ICA for nonstationary signals using Rough–fuzzy, c-means clustering .[13] The focus was on extraction of damage features from short-term, nonstationary, external excitations that potentially occur at discrete single intervals, such as during passage of heavy truck or train across a bridge. Although the methodology was sound, ICA required complicated and time-consuming, algorithmic solutions.

2.1 | Physical interpretations of POD

Close connections between POMs and natural eigenmodes of mechanistic systems have been established.[54,55] Theoretical and experimental research has also attempted to link POMs to linear and nonlinear mechanical system eigenmodes.[56,57] A recent study focused on the potential of POD as a modal identification tool and concluded that system mass distribution is required in general cases.[58]

Free vibrations of an undamped linear system having a mass matrix proportional to the identity matrix were shown to provide POMs that asymptotically converged to its eigenmodes.[55] POMs of a lightly damped similar system were shown to closely estimate its eigenmodes, except for forced harmonic vibrations.[55] Findings also showed that, independent of system mass, POMs could coincide with eigenmodes for certain resonant frequencies.[59] North established a general criteria relating POMs to eigenmodes for mechanical systems excited by noise.[60]

The research work summarized above supports the premise that mass-weighted POMs converge to eigenmodes for structural systems subjected to broadband excitations. This means that POMs of structural response to white noise are primarily a function of system properties, not imposed loads. Conversely, when loads having strong harmonic frequencies are applied to a structure, resulting POMs depend both on the structure's mechanistic properties and on frequency content of the applied excitation. Therefore, when using POMs as damage features, one should analyze uncertainties of the POMs via propagating uncertainties of operational loads and structural deficiencies.

2.2 | PCA and SVD as POD methods

PCA looks for the subspace that features maximum data series variability when attempting to discover core dependency structures within that data. This can be interpreted as, in a state-space domain, directions in which data variability is important representing prevailing directions where system dynamics response is occurring, whereas directions featuring no data variability are redundant with respect to representing dynamic response. When dealing with a structural system, those directions are akin to its eigenvectors, which depend only on system properties. In this case, the principal subspace is purely statistical and is a function of external excitations and mechanistic properties of the system.

Consider the vector $\boldsymbol{u} \in \mathbb{R}^m$, where this vector could represent measured structural response or any other system variable. Suppose $y_1, y_2, \ldots, y_m \in \mathbb{R}$ are the first, second, and m^{th} principal components of $\boldsymbol{u}$. Let the first principal component, y_1, be a linear combination of each element of the original vector:

$$y_1 = \sum_{i=1}^{m} \xi_{i1} u_i = \boldsymbol{\xi}_1^T \boldsymbol{u}, \tag{1}$$

where $\boldsymbol{\xi}_1$ is a coefficient vector containing linear combinations of principle components, and $\boldsymbol{\xi}_1 = \{\xi_{11}, \xi_{21}, ..., \xi_{m1}\}^T$. It can be assumed that each column of the snapshot matrix (the matrix in which samples of structural response or any other system variable are collected) of Equation 1 is a linear combination of principle components and principal vectors, $\boldsymbol{\xi}_j$, $j = 1, 2, ..., m$, as shown in Equation 2. Therefore, an objective of PCA could be expressed as finding the first principal vector $\boldsymbol{\xi}_1$ such that, when one projects all individual columns of the snapshot matrix onto it, resulting values, denoted by $y_1^1 \cdots y_1^n$, would feature maximum variance. The second principal vector, $\boldsymbol{\xi}_2$, features projected values, $y_2^1 \cdots y_2^n$, having the second highest variance and so on.

$$\begin{aligned}
\begin{bmatrix} \boldsymbol{u}_1 \end{bmatrix}_{m\times 1} &= y_1^1 \begin{bmatrix} \boldsymbol{\xi}_1 \end{bmatrix}_{m\times 1} + y_2^1 \begin{bmatrix} \boldsymbol{\xi}_2 \end{bmatrix}_{m\times 1} + \cdots + y_r^1 \begin{bmatrix} \boldsymbol{\xi}_r \end{bmatrix}_{m\times 1} + ... + y_m^1 \begin{bmatrix} \boldsymbol{\xi}_m \end{bmatrix}_{m\times 1} \\
\begin{bmatrix} \boldsymbol{u}_2 \end{bmatrix}_{m\times 1} &= y_1^2 \begin{bmatrix} \boldsymbol{\xi}_1 \end{bmatrix}_{m\times 1} + y_2^2 \begin{bmatrix} \boldsymbol{\xi}_2 \end{bmatrix}_{m\times 1} + \cdots + y_r^2 \begin{bmatrix} \boldsymbol{\xi}_r \end{bmatrix}_{m\times 1} + ... + y_m^2 \begin{bmatrix} \boldsymbol{\xi}_m \end{bmatrix}_{m\times 1} \\
&\vdots \\
\begin{bmatrix} \boldsymbol{u}_n \end{bmatrix}_{m\times 1} &= y_1^n \begin{bmatrix} \boldsymbol{\xi}_1 \end{bmatrix}_{m\times 1} + y_2^n \begin{bmatrix} \boldsymbol{\xi}_2 \end{bmatrix}_{m\times 1} + \cdots + y_r^n \begin{bmatrix} \boldsymbol{\xi}_r \end{bmatrix}_{m\times 1} + ... + y_m^n \begin{bmatrix} \boldsymbol{\xi}_m \end{bmatrix}_{m\times 1}.
\end{aligned} \tag{2}$$

The variance of y_1, assumed to be a random variable, is then[50]

$$S_{y_1}^2 = \boldsymbol{\xi}_1^T \boldsymbol{Z}_u \boldsymbol{\xi}_1, \tag{3}$$

where $\boldsymbol{Z}_u$ the covariance of the variable $\boldsymbol{u}$, is assumed to be random as well. A maximum value for $S_{y_1}^2$ would not be achieved for a finite value of $\boldsymbol{\xi}_1$ so, a constraint would have to be imposed as follows:

$$\max_{\boldsymbol{\xi}_1} \left(\boldsymbol{\xi}_1^T \boldsymbol{Z}_u \boldsymbol{\xi}_1 \right), \text{ such that } \left(\boldsymbol{\xi}_1^T \boldsymbol{\xi}_1 \right) = 1. \tag{4}$$

By using the Lagrangian multiplier, λ_1, to numerically constrain the optimization problem, Equations 3 and 4 yield

$$L(\boldsymbol{\xi}_1, \lambda_1) = \boldsymbol{\xi}_1^T \boldsymbol{Z}_u \boldsymbol{\xi}_1 + \lambda_1 \left(1 - \boldsymbol{\xi}_1^T \boldsymbol{\xi}_1 \right), \tag{5}$$

where $L(\blacksquare)$ is a Lagrangian operator. By differentiating this objective function with respect to the first principal direction, $\boldsymbol{\xi}_1$, and finding the root of the resulting derivative, it can be shown that

$$\frac{\partial L(\boldsymbol{\xi}_1, \lambda_1)}{\partial \boldsymbol{\xi}_1} = 2(\boldsymbol{Z}_u - \lambda_1 \boldsymbol{I})\boldsymbol{\xi}_1 = 0 \Rightarrow \boldsymbol{Z}_u \boldsymbol{\xi}_1 = \lambda_1 \boldsymbol{\xi}_1, \tag{6}$$

where λ_1 and $\boldsymbol{\xi}_1$ are the eigenvalue and the corresponding eigenvector of the covariance matrix $\boldsymbol{Z}_u$, respectively, and direct equality between the covariance matrix and system eigenvalues is established.

By following similar procedure, the objective function to be maximized in order to extract the i^{th} principal component and vector of a random variable appears as

$$\max_{\boldsymbol{\xi}_i} \left(\sum_{i=1}^{m} \boldsymbol{\xi}_i^T \boldsymbol{Z}_{\boldsymbol{u}} \boldsymbol{\xi}_i \right), \text{ such that } \left(\boldsymbol{\xi}_i^T \boldsymbol{\xi}_j \right) = \delta_{ij}. \tag{7}$$

To compute its principal components, one must populate a covariance matrix for a multivariate, random process. However, in practice, it is usually impossible to determine this covariance matrix, and it is a common practice to

approximate it using a correlation matrix.[61] To approximate the covariance matrix with a reasonable level of accuracy, one needs an appropriately chosen sample set, in the snapshot matrix. In context of structural dynamics, matrix columns represent the system state at a specific instance in time. The covariance of the data set, represented in snapshot matrix $\boldsymbol{U}$, is calculated as[61]

$$\boldsymbol{Z}_u = \lim_{n\to\infty}\left(\widetilde{\boldsymbol{Z}}_u = \frac{1}{n}\boldsymbol{U}\boldsymbol{U}^T\right). \tag{8}$$

A straightforward way to obtain eigenvectors and eigenvalues of the corresponding correlation matrix is to apply SVD to this snapshot matrix. Applying SVD to the snapshot matrix $\boldsymbol{U} = \boldsymbol{L}\,\boldsymbol{\Sigma}\,\boldsymbol{R}^{\mathrm{T}}$, gives, using Equation 8:

$$\mathbf{Z} = \frac{1}{n}\boldsymbol{U}\boldsymbol{U}^T = \frac{1}{n}\boldsymbol{L}\boldsymbol{\Sigma}\boldsymbol{R}^{\mathrm{T}}\boldsymbol{R}\boldsymbol{\Sigma}\boldsymbol{L}^T = \frac{1}{n}\boldsymbol{L}\boldsymbol{\Sigma}^2\boldsymbol{L}^T \tag{9}$$

Multiplying both sides of Equation 9 by $\boldsymbol{L}$, it can be deduced that the eigenvectors of $\mathbf{Z}$ are singular vectors of the snapshot matrix:

$$\mathbf{Z}\,\boldsymbol{L} = \frac{1}{n}\boldsymbol{L}\boldsymbol{\Sigma}^2, \tag{10}$$

and corresponding eigenvalues are diagonal components of $\frac{1}{n}\boldsymbol{\Sigma}^2$.

3 | ANNS FOR SNAPSHOT MATRIX CLASSIFICATION, POM REGRESSION, AND DAMAGE IDENTIFICATION

As stated earlier, ANNs have been extensively studied in association with structural damage identification, with feed forward architecture being the most prevalent technique. The current study explores the use of two-stage ANNs for structural damage identification, as outlined in Figure 1. In the first stage, a classification ANN is employed to assign the snapshot matrix to a certain response category. In the second stage, an ANN is trained for nonlinear regression to a set of POMs and their associated damage indexes. The resulting POMs are subsequently used to identify damage.

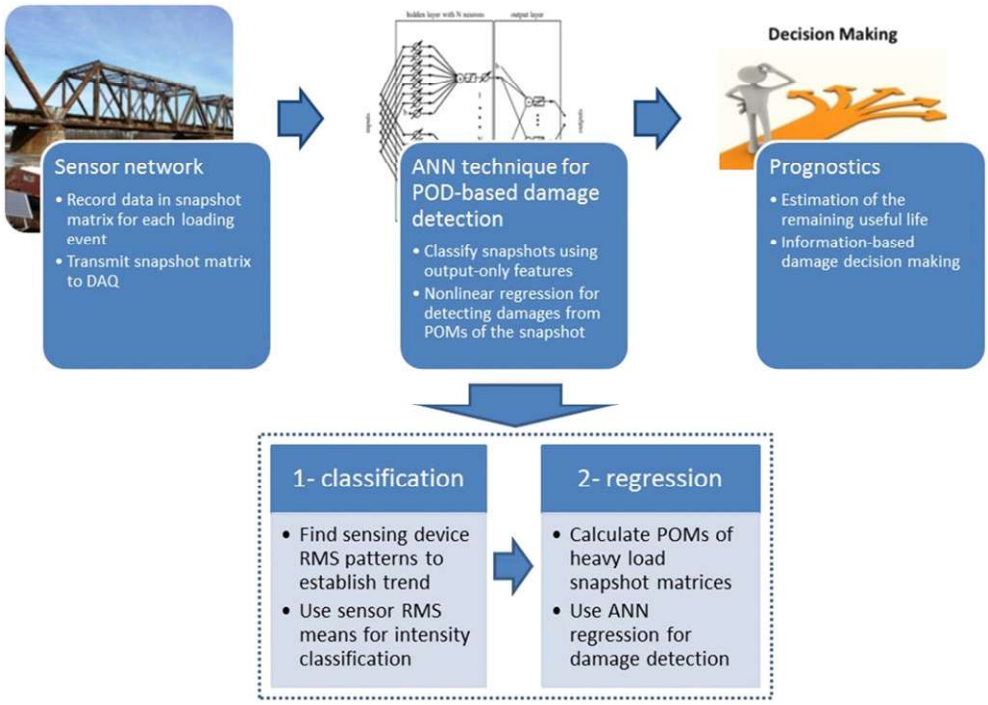

FIGURE 1 Proposed nonlinear, two-layer, ANN technique for Proper Orthogonal Decomposition-based damage detection

MATLABs Neural Network Toolbox was used for data analysis and constructing the classification and regression networks.[62]

3.1 | Nonlinear regression using ANNs

ANN regression and classification models were constructed based on a linear combination of predetermined nonlinear basis functions $\varphi_j(\mathbf{x})$[63]:

$$\boldsymbol{y}(\mathbf{x},\mathbf{w}) = f\left(\sum_{j=1}^{M} w_j\, \varphi_j(\mathbf{x})\right), \tag{11}$$

where $f(\blacksquare)$ is a nonlinear activation function in the case of classification, however, in case of regression, equals identity. A two-layer feed forward neural network was adopted for both regression and classification tasks carried out in this study. This architecture has been shown to approximate arbitrary nonlinear functions well.[64,65] The relationship between input and the j^{th} component of the output of this type of ANN is given by[63]

$$y_k(\mathbf{x},\mathbf{w}) = \sigma\left(\sum_{j=1}^{M} w_{kj}^{(2)}\, h\left(\sum_{i=1}^{D} w_{ji}^{(1)}\, x_i + w_{j0}^{(1)}\right) + w_{k0}^{(2)}\right). \tag{12}$$

Where $\mathbf{y} \in \mathbb{R}^{\mathrm{K}}$ is the output vector; $\mathbf{x} \in \mathbb{R}^{\mathrm{D}}$ are inputs for the neural network; M denotes the number of neurons in the hidden layer; $w_{kj^{(2)}}$ and $w_{k0^{(2)}}$ represent weights and biases of the output layer; and $w_{ji^{(1)}}$ and $w_{j0^{(1)}}$ represent weights and biases of the hidden layer. In this study, a hyperbolic tangent sigmoid activation function, $h(\blacksquare)$, is employed as the hidden layer activation function. The activation function for the regression output layer $\sigma(\blacksquare)$ is represented by the identity matrix except in the case of multiclass problems, where a softmax activation function is used.[63]

Supervised training was used with Bayesian regularization being implemented to distinguish between noise and the hidden data structure.[64] Given that a regression output layer was being considered, the most common objective function was the least mean-squared error[66]:

$$\mathrm{E}^d = \sum_{\mathrm{k}=1}^{\mathrm{N}} \left\|\mathbf{t}_{\mathrm{k}} - \mathrm{y}_{\mathrm{k}}(\mathbf{x}_{\mathrm{k}},\mathbf{w})\right\|^2, \tag{13}$$

Where $\{\mathbf{x}_{\mathrm{k}}\}$ ($k = 1, 2, \ldots, N$) were input vectors, and their corresponding target values were $\{\mathbf{t}_{\mathrm{k}}\}$, with d referring to data. The regularization adds another term to the objective function:

$$\mathrm{E} = \beta\, \mathrm{E}^d + \alpha\, \mathrm{E}^w, \tag{14}$$

where E^w is the sum of square root of network weights; w refers to those weights; and α and β are objective function parameters. The ratio of objective function parameters determines the training emphasis with larger α/β pushing the network towards generalization and smaller ratios driving the network towards error minimization.[67]

4 | COUPLED POM AND ANN OUTPUT-ONLY DAMAGE DETECTION: APPLICATION TO A DOUBLE-TRACK, RAILWAY TRUSS BRIDGE

The proposed, coupled POD and ANN framework were validated using simulated experiments analyzing the response of an existing railway bridge using FE models subjected to recorded train loads from weigh-in motion (WIM) stations near the bridge site. This investigation not only served to help substantiate the proposed framework but also helped assess the viability of implementing an optimized network of strain sensors for online and real-time damage detection on a full-scale structure. The FE model was developed in SAP2000[68] based on design drawings. Measured train axle loads traversed the model, and structural response to live loads was examined by studying strain time histories. Measurement uncertainty was represented using zero mean, white Gaussian noise superimposed onto the strain time histories.

The bridge under study is located on a heavily used freight rail corridor in central Nebraska and is an open deck, double-track structure consisting of five, single-span, steel Warren trusses and six, single-span steel, through girder

approach spans (Figure 2). The total length of the bridge is 381.0 *m* with the studied truss span have on overall length of 45.5 *m*. An elevation and plan view of the examined truss span and the proposed instrumentation locations are shown in Figure 3. A numerical sensitivity analysis was completed by Rageh[69] on the structure considered in this article, to quantify the change in strains time histories at a set of instrumented locations due to deficiencies. To this end, most common deficiency types at arbitrary locations of the bridge were selected. The study concluded that using 20 sensors at locations assumed in this study would be the smallest set of sensors needed for detecting stringer-to-floor beam damages. See the Appendix for further details on the bridge structure.

A parametric study using the model was completed to examine POM variations as a function of changes in (1) non-stationary excitations caused by moving trains and (2) structural defect locations and levels. Linear time history analyses were performed, and zero-mean white Gaussian noise was added to resulting strain time histories to yield a noise to

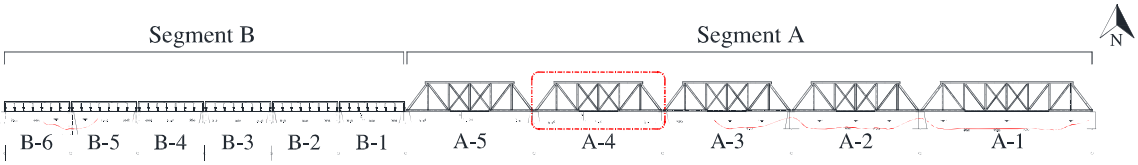

FIGURE 2 Bridge elevation looking north. The studied span is marked with a red rectangle

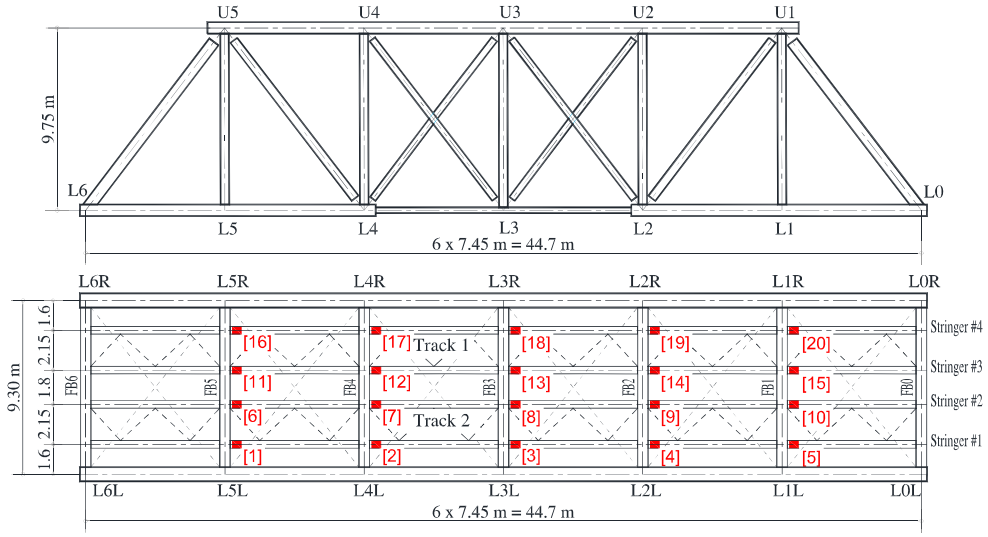

(a)

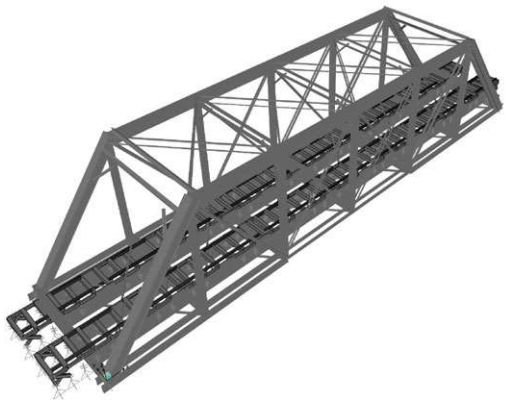

(b)

FIGURE 3 Studied truss span (a) elevation view and plan views denoting finite element method "sensor" (FEM nodes reporting strain time history) locations, (b) isometric view of the 3D finite element method model created in SAP2000

signal ratio of 1%. It was assumed that dynamic strains were "measured" at a frequency of 50 *Hz*. WIM data for 81 trains was used for the FE simulations, with this data being assumed to statistically represent the distribution of train loads under operational conditions. Inertial interactions between train cars and the bridge were neglected. Any kind of sensor (e.g., accelerometers) could be potentially used within the proposed framework. However, strain sensors provide a more direct means of monitoring certain deficiencies, such as fatigue damage. Moreover, strain measurements can provide more sensitivity to local changes in structural response. Limited live load damping occurs when dealing with open-deck railway bridge systems whose rails and ties are directly placed onto the superstructure. Consequently, significant localized impact dynamics are observed in structural members, which, in turn, can adversely affect damage detection capabilities if accelerations would be used to track structural response. Separating local from global dynamics to facilitate damage detection is not a trivial task and was not within the scope of this study.

4.1 | Nonstationary excitation influence on POMs

Examination of nonstationary excitation sensitivity was initially studied by looking at the effect of train speed on POMs, with the POMs developed based on strain time-history information as detailed below ("output"). A representative surface plot, one that shows changes in values for components of the first POM of each snapshot matrix at different "sensor" locations (FEM nodes reporting strain time-histories) with respect to a reference train speed, is shown in Figure 4 for a healthy bridge. For this case, 50 mph was chosen as the reference train speed, and surface plots are presented as the algebraic difference between POM components at 25 and 75-mph speeds. Different colors in the surface plots are arbitrarily associated with different POM component magnitudes and surface slopes. POMs were initially extracted at different train speeds using a fixed length snapshot matrix, a common POD data reduction practice. The plots indicate that POMs change as a function of train speed. At this point, it should be stated that POD is a statistical tool for extracting directions in a variable space that best capture data variability. For the random variable being studied (a vector including temporal magnitude of strain at a network of sensors), POMs are a function of samples taken from those variables. To reduce changes in POMs when dealing with snapshot matrices associated with trains with different speeds, samples in the snapshot matrix were chosen so that they featured the same number of "sensor" strain peaks during train passage utilizing an automated peak-picking algorithm available in MATLAB.[70] As evidenced by plots in Figure 5, including the same number of peaks in samples for snapshot matrix could visibly reduce the variability of POMs caused by change in train speed.

POM sensitivity to nonstationary excitations was further examined by varying train transverse location (i.e., passage on different tracks) and train load, with results shown in Figure 6. It was observed that transverse load position had substantial effect on POMs, results that will be further examined below.

Load effects were examined using two extreme cases, one for the train having the highest statically equivalent uniform axle load ("heavy") and one for the train having the lowest statically equivalent uniform axle load ("light"). POMs were shown to be largely unaffected by train load.

When studying effects of speed on POMs, it was observed that peak picking can help reduce POM dispersion. Utilizing peak picking helped categorize snapshot matrices and subsequently reduce POM variability resulting from train load variability. After peak picking, the 81 trains involved in the study were sorted using strain time history root mean squares (RMSs) measured by the 20 sensors shown in Figure 3. The resulting, sorted, train RMS data are shown in numerical order by sensor number in Figure 7 along with accompanying statically equivalent uniform loads. Bars are nondimensionalized with respect to maximum RMS and statically equivalent loads for the 81 trains. These results demonstrate strong correlation between statically equivalent uniform loads (input) and RMSs of resulting strain time-history snapshot matrices measured from each train passage (output). To examine POM variability in snapshot matrices having

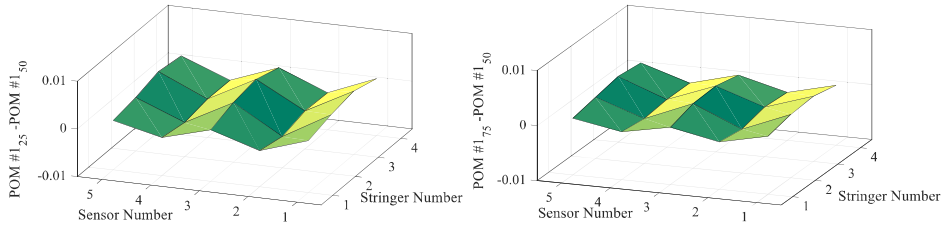

FIGURE 4 Three-dimensional strain time history POM at various train speeds using fixed-length snapshot matrices

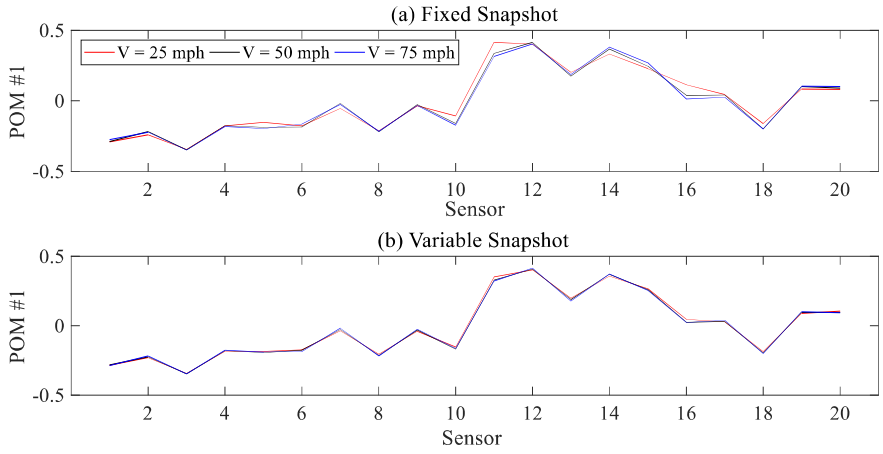

FIGURE 5 Two-dimensional strain-time history proper orthogonal modes at various train speeds using (a) fixed-length and (b) variable-length snapshot matrices

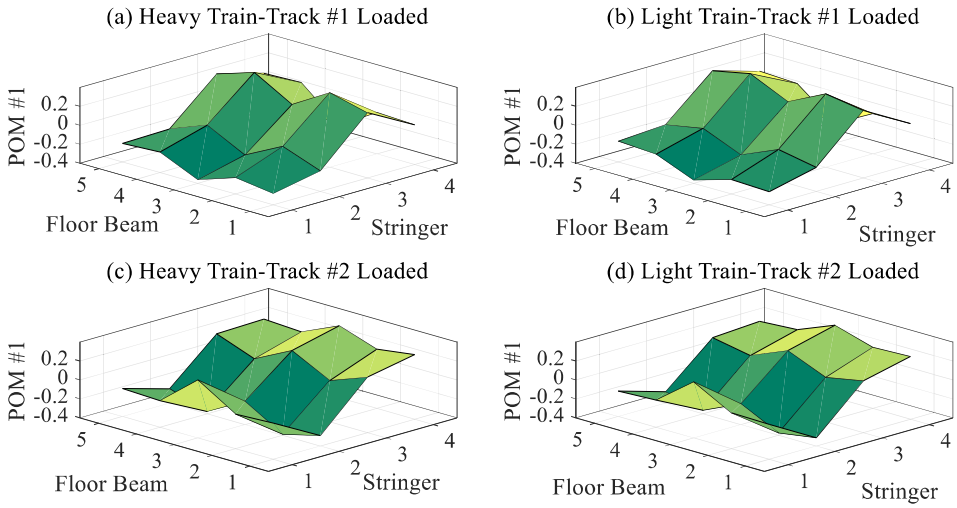

FIGURE 6 Three-dimensional strain-time history proper orthogonal modes for heavy and light train on Tracks 1 and 2

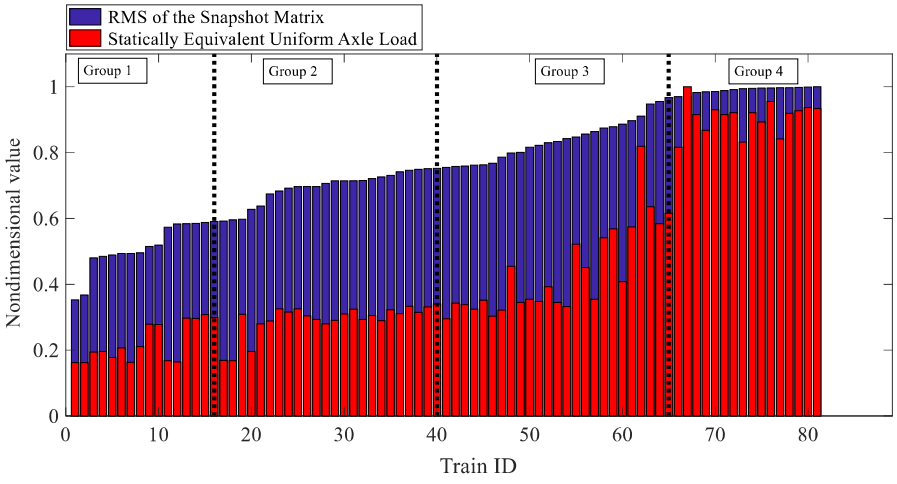

FIGURE 7 Trains sorted by strain nondimensionalized time-history snapshot matrix root mean square with corresponding nondimensionalized statically equivalent uniform load

relatively close RMS values, trains were arbitrarily divided into four groups based on RMS as denoted by the vertical black dashed lines in Figure 7. Group 1 (lowest RMS) included 16 trains; Group 2, 24 trains; Group 3, 25 trains; and Group 4, 16 trains. POMs for each group are shown in the 2D plots in Figure 8, with Group 4 having the best correlation. To further study if output-only POMs were truly unaffected by system inputs, Group 4 POM means and standard

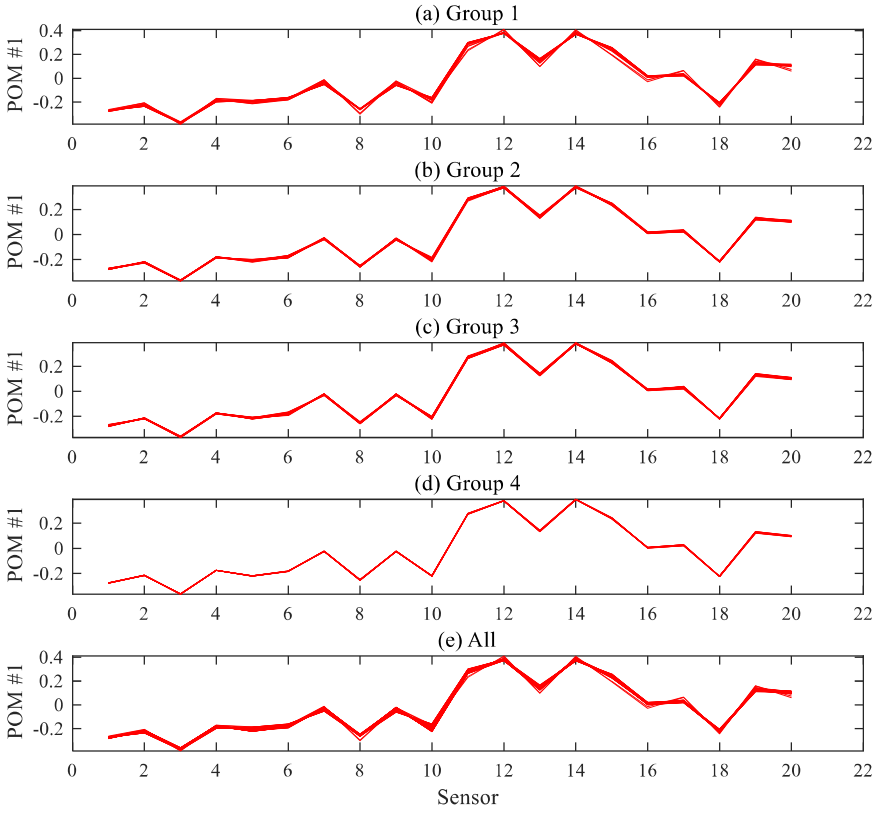

FIGURE 8 Two-dimensional proper orthogonal modes plotted by Figure 7 group number

deviations were compared with similar POMs for all trains at each of the 20 sensor locations, with results shown in Figure 9. It can be observed that, whereas the means were very similar, POMs associated with trains developing high strains and RMS values had lower standard deviations (i.e., less dispersion).

It should be noted that an optimal selection of the number of RMS groups to minimize axle load variability is a function of various parameters, such as the duration of the training period, acceptable damage estimation error, and environmental variability at the bridge site. The effects of these items on optimal output-only categorization of response snapshots is being examined as part of a companion study.

Given its low-RMS standard deviation, Group 4 allowed for efficient training of a regression-based ANN, with the ANN being used to link the first POM of the snapshot matrices to damage indices. A supervised learning approach was adopted for classification of structural response snapshots, which, in turn, would be used to categorize the snapshot matrices and assign them to each RMS group based on sensor measurement features. To this end, RMS snapshot matrix means were selected features for all sensors in the snapshot matrix. Using this feature and randomly selecting 70% of available samples for training, 15% for validation and 15% for testing, an ANN-based classifier was established to help

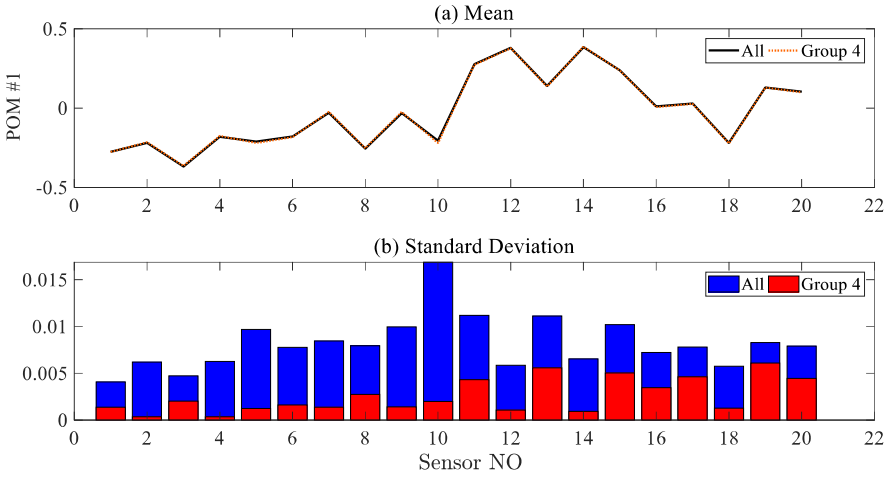

FIGURE 9 Proper orthogonal modes means and standard deviations for all trains and group 4 from Figure 7

determine the weighting group to which the snapshot matrix belonged. A classifier confusion matrix,[71] where columns of the matrix represent target groups and rows show output for the classification task, was used to measure how "confused" a classifier is during evaluation and testing for a given set of training data. The resulting confusion matrix is shown in Figure 10 for each feature set. Numbers in the green cells represent correct classification using the classifier whereas red cells quantify incorrect classifications. Given that the figure shows 0% error in the gray, red, and blue cells, labels are correctly assigned to each response snapshot for the training, testing, and entire sample sets. Subsequently, the ANN-based classifier can be effectively employed for categorization of the inputs (train loads) based purely on output measurements ("sensor" strains). In addition to identifying train loads based solely on measured strain time histories, RMS signal ratios can automatically be employed to determine which track was loaded.

It should be highlighted that, in the present case, categorization was pursued in one dimension, and error was expected to be low. Instead of using ANNs to categorize the snapshot matrices, predefined intervals could be adopted for input classification based on measured response. Authors adopted ANNs for present study framework because of their versatility when dealing with more complicated categorization tasks, such as those that include environmental variability.

4.2 | Measurement noise influence on POMs

One of the most important features in any SHM framework is robustness to noise. To address any potential noise issues, novel damage detection frameworks are tested for sensitivity to elevated noise intensities. Simoen et al. proved that spatial correlation of measurement noise could affect certain damage detection frameworks.[72] The current study examined effect of measurement noise intensity and spatial correlation on POMs. It has to be stated that, in all analyses

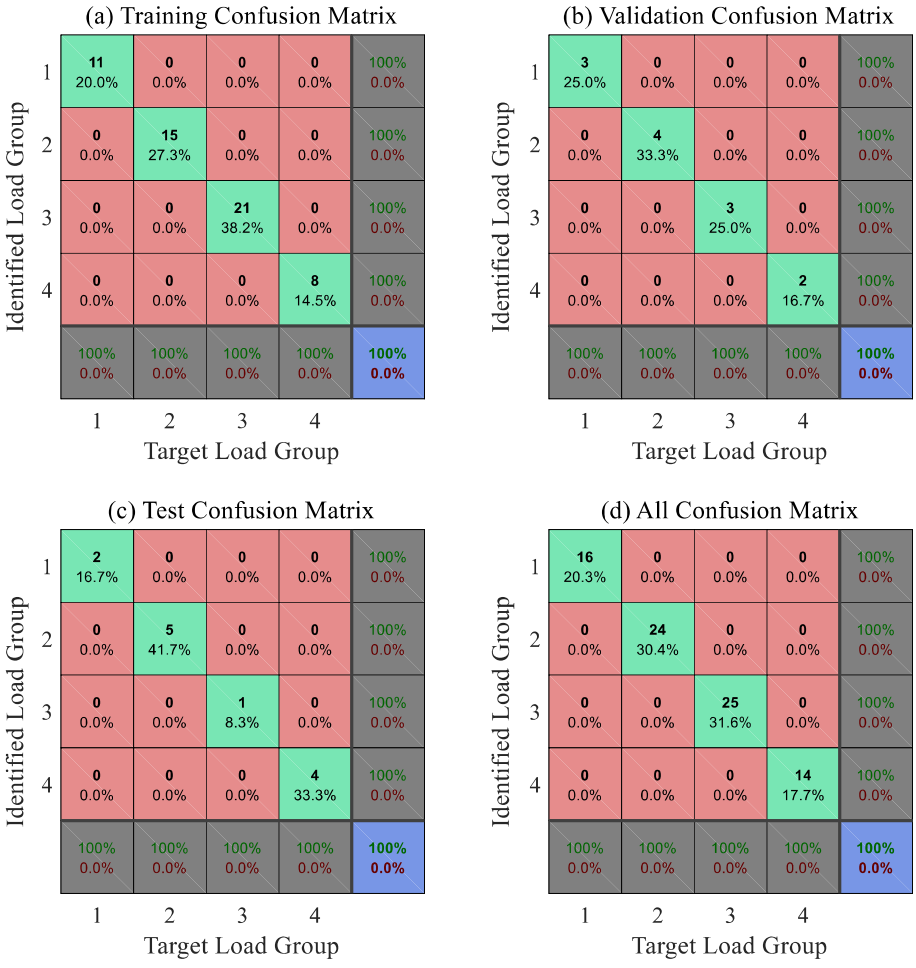

FIGURE 10 ANN-based classifier confusion matrix

carried out, herein, noise was temporally uncorrelated. Figure 11 depicts snapshot matrix POMs obtained from four loading scenarios. Spatially uncorrelated noise was considered using 10 and 15% RMS noise to signal ratios, and extracted POMs were compared with reference signals. In Figure 12, the noise was spatially correlated. As seen in Figures 11 and 12, POMs were shown to be robust against both elevated noise levels and spatial correlation.

4.3 | Structural deficiency influence on POMs

Al-Emrani[73] studied the behavior of double-angle, stringer-to-floor-beam connections in riveted railway bridges by performing tests on three full-scale bridge members taken from a decommissioned, riveted railway bridge. It was concluded that the corresponding reduction in rotational stiffness caused by fatigue crack propagation equaling 40%

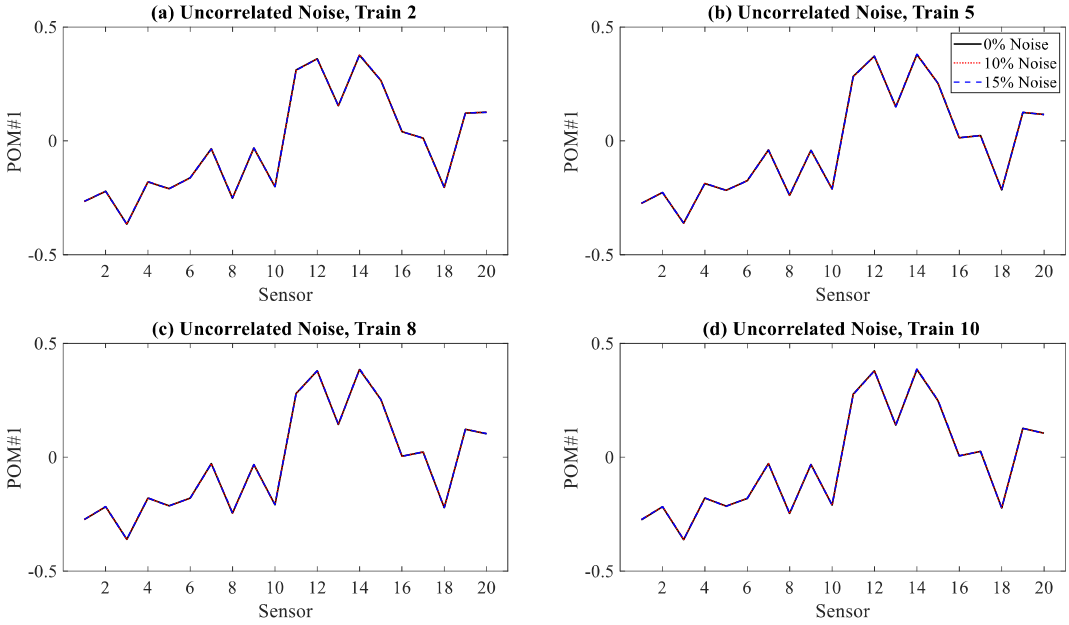

FIGURE 11 Spatially uncorrelated proper orthogonal modes at various noise intensities

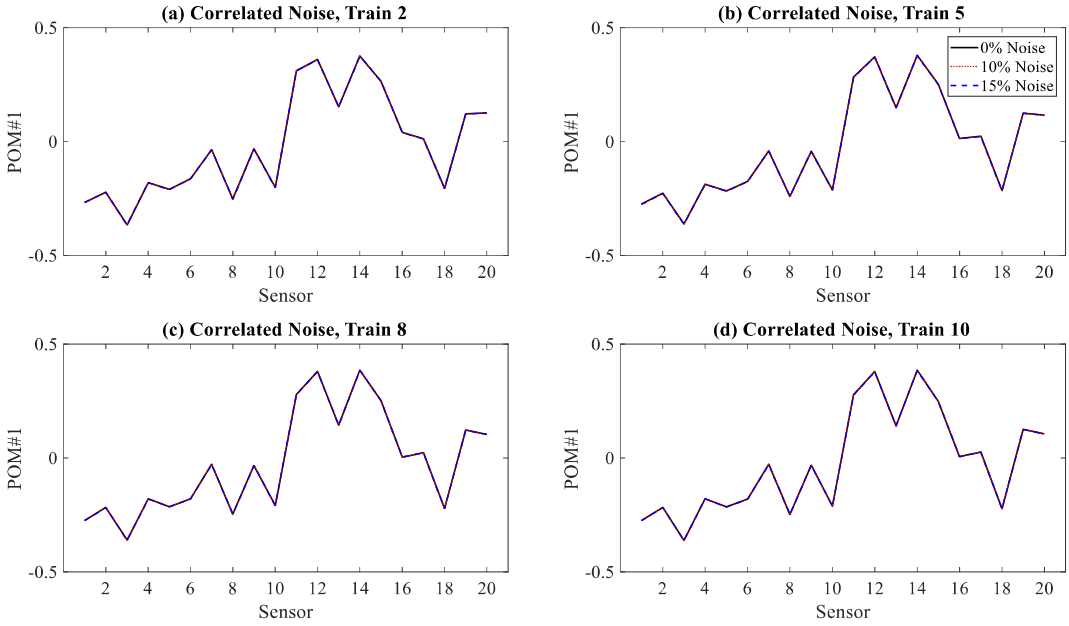

FIGURE 12 Spatially correlated proper orthogonal modes at various noise intensities

of the connecting angle leg length was approximately 65% of the rotational stiffness of an uncracked leg. For the current study, structural deficiency influence on POMs was initially investigated by reducing stringer-to-floor-beam rotational stiffness to mimic fatigue crack development their connections. Stiffness reductions that encompassed values reported by Al-Emrani,[73] ranging between 20 and 80%, were selected. Resulting changes in POMs were examined by comparing difference of POMs of the intact and damaged structure, as shown in Figure 13 for a single-loading event. This representative comparison demonstrates that 25 and 50% stiffness reductions were distinctly identified by the POMs and distinctly varied as damage increased. These findings were consistent and independent of transverse train location (i.e., loaded track), results that indicated that damage at locations away from highly loaded areas could be identified. POMs for the healthy bridge under 10 heavy train passes were compared with those for a bridge having deficient connections under the same train loads, with results shown in Figure 14. For stiffness reductions of 20, 40, and 60% minimal changes to resulting POMs were observed. At 80% stiffness reduction, a change was observed for POMs at the damage location. This indicates that critical levels of damage could be intuitively detected from POMs; however, small deficiencies could be overlooked. When structures are subjected to stationary loads, small-damage levels could be detected by merely

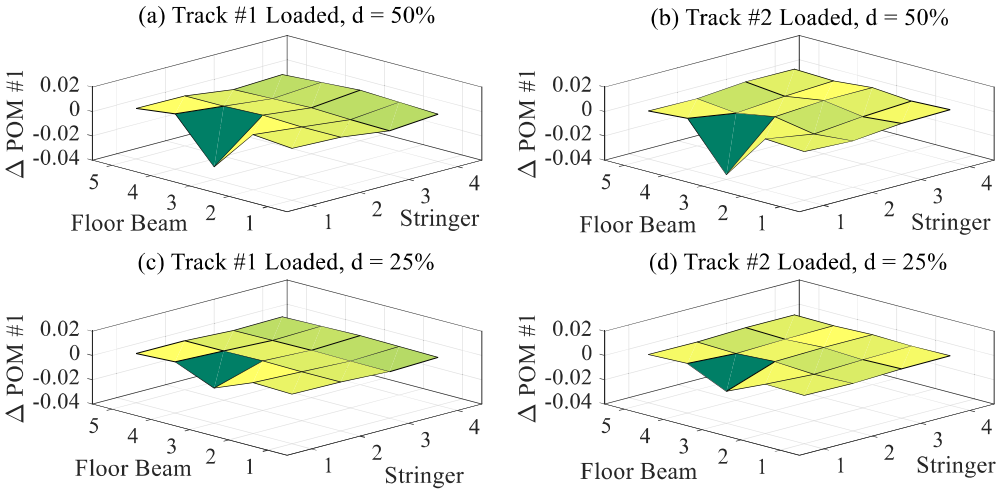

FIGURE 13 Difference in proper orthogonal modes for (a) $\boldsymbol{d = 50}$% damage to a connection, load on track #**1**, (b) $\boldsymbol{d = 50}$% damage to a connection, load on track #**2**, (c) $\boldsymbol{d = 25}$% damage to a connection when track #**1** loaded, and (d) $\boldsymbol{d = 25}$% damage to a connection when track #**2** loaded, on a connection in vicinity of stringer #**1**, sensor #**3**, where $\Delta \mathbf{POM} = \mathbf{POM}_{\mathbf{before\ deficiency}} - \mathbf{POM}_{\mathbf{after\ deficiency}}$

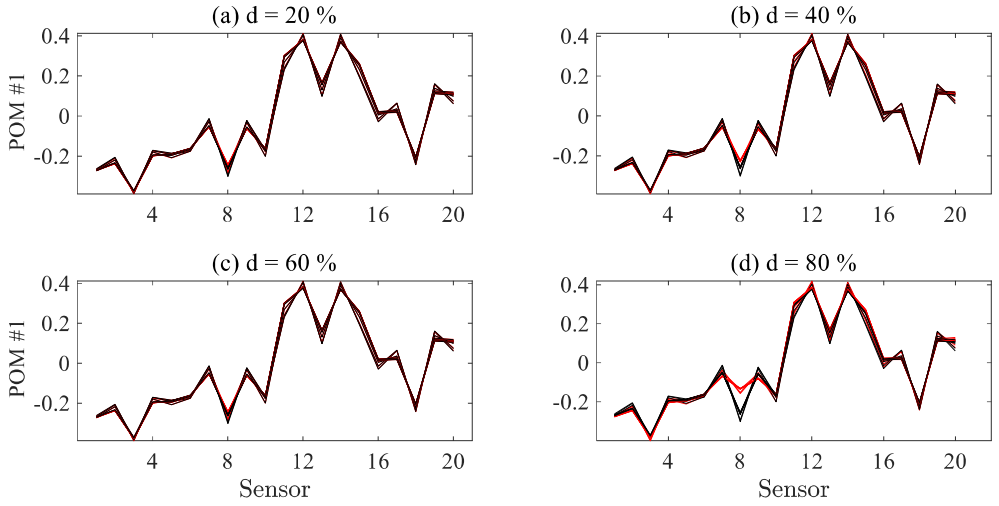

FIGURE 14 Proper orthogonal modes of a healthy bridge for 10 heavy train passages scenarios compared with (a) $\boldsymbol{d = 20}$% damage to a connection in vicinity of sensor #**8**, (b) $\boldsymbol{d = 40}$% damage to a connection in vicinity of sensor #8, (c) $\boldsymbol{d = 60}$% damage to a connection in vicinity of sensor #**8**, and (d) $\boldsymbol{d = 80}$% damage to a connection in vicinity of sensor #**8**. Red lines = deficient cases, and black lines represent healthy cases

analyzing POMs before and after loading, as seen in Figure 13. This observation substantiates the need for a more advanced method for damage identification when POMs are defined as the damage features for variations in train axle loads affect the adopted damage features. To deal with that issue, ANNs were trained to systematically detect damages based on calculated POMs in each loading scenario.

4.4 | ANNs for damage detection

To further investigate POM sensitivity to damage, particularly for damage intensities lower than **20**% where POM changes could be overlooked when the loading source is nonstationary, an ANN-based regression of damage indices to POMs was completed. A set of nine heavy trains were randomly selected from Group #4 (see Figure 7) and were used to generate strain time histories for damage between 10 and 100% reductions in rotational stiffness in the vicinity of all individual "sensors" shown in Figure 3. This approach produced 200 damage scenario POMs for a given train load, with POMs for the healthy structure also included in the training data set. One hundred neurons were used in the ANN hidden layer and, when subjected to nine train loads, the input data set totaled 1,809 POMs for supervised training of the feedforward regression network with 1,809 damage index vectors being training outputs. A flowchart of the procedure is shown in Figure 15.

ANN-based regression helped establish the protocol for identifying damage using these POMs. As had occurred previously, 70% of the samples were selected for training, 15% for validation, and 15% for testing. Figure 16 provides correlation curves for the training, testing, and entire input data sets, with circles representing the magnitude of the estimated damage index. Ideal correlation is represented by the dashed line whereas colored lines represent a linear fit that minimizes least-squares error for predicted damage indices. It should be highlighted that the estimated correlation line is superimposed on ideal correlation and is not visible in the plots. This indicates that ANN-based regression accurately predicted damages having various intensities. One train load case was not used to develop the regression function and was adopted for further testing of the accuracy of the proposed damage detection technique. Figure 17 depicts results for

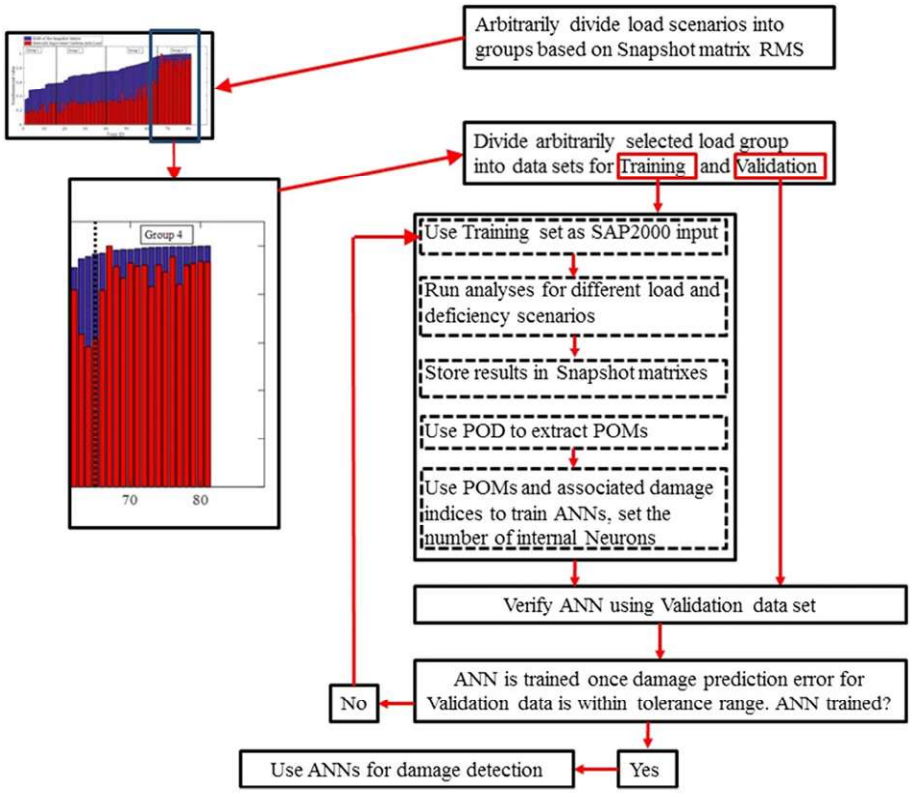

FIGURE 15 Process for selecting train loads and training and validation artificial neural networks

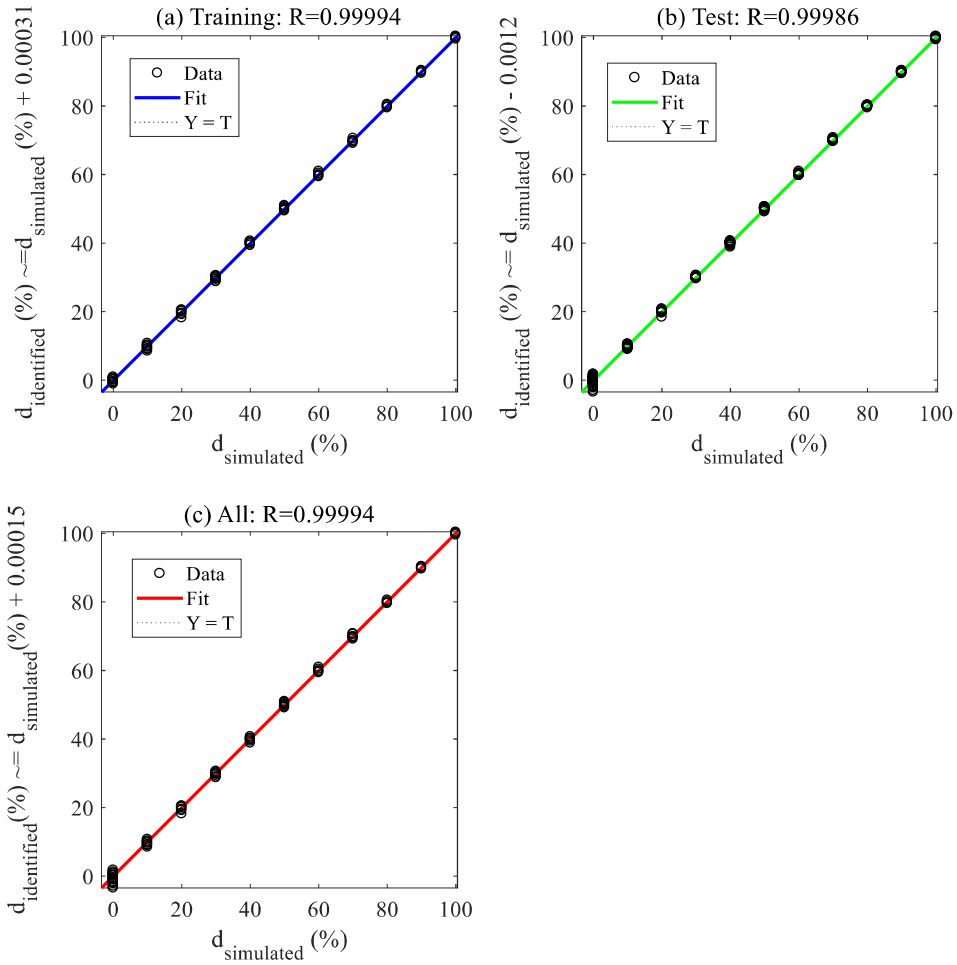

FIGURE 16 Correlation between artificial neural network output and target values, training, tests and entire datasets

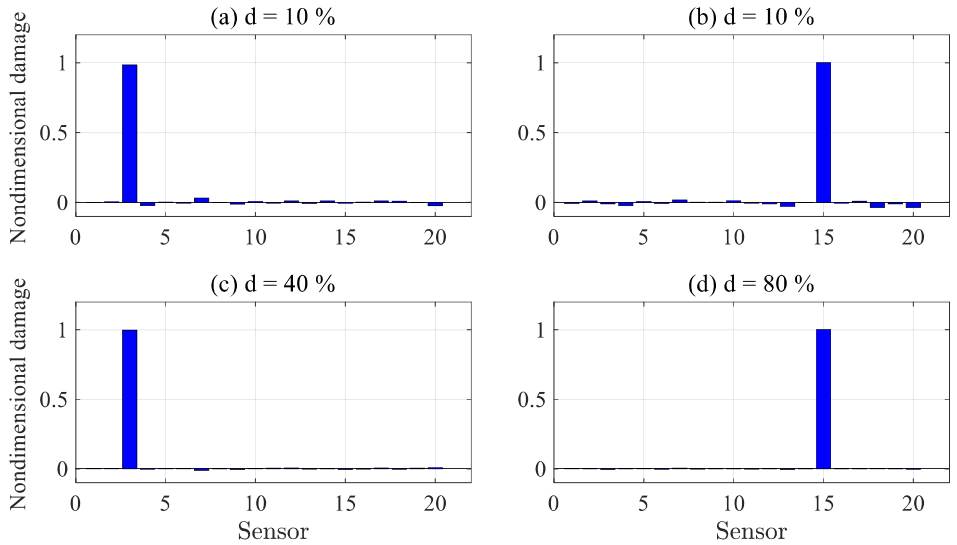

FIGURE 17 Nondimensionalized damage indexes from artificial neural network regression for (a) $\boldsymbol{d = 10}$% damage to a connection in vicinity of Sensor **3**, (a) $\boldsymbol{d = 10}$% damage to a connection in vicinity of Sensor **15**, (c) $\boldsymbol{d = 40}$% damage to a connection in vicinity of Sensor **3**, and (d) $\boldsymbol{d = 80}$% damage to a connection in vicinity of Sensor **15**

this case, plotting nondimensionalized damage estimates for stiffness reductions of 10%, 40%, and 80% at sensor locations #3 and #15 in Figure 3. The figure shows that, for the three damage intensities, negligible estimation error existed with error levels decreasing at higher damage levels. A more intuitive tool was developed to help end users determine where damage was predicted on the bridge floor system, with examples being shown in Figure 18 for damage intensities ranging from 20 to 100%. This "heat map" overlays identified damage index vectors onto a plane representing the floor system and, ultimately, "sensor" locations, and provided another way to confirm that ANN regression accurately identified damage regardless of location and intensity.

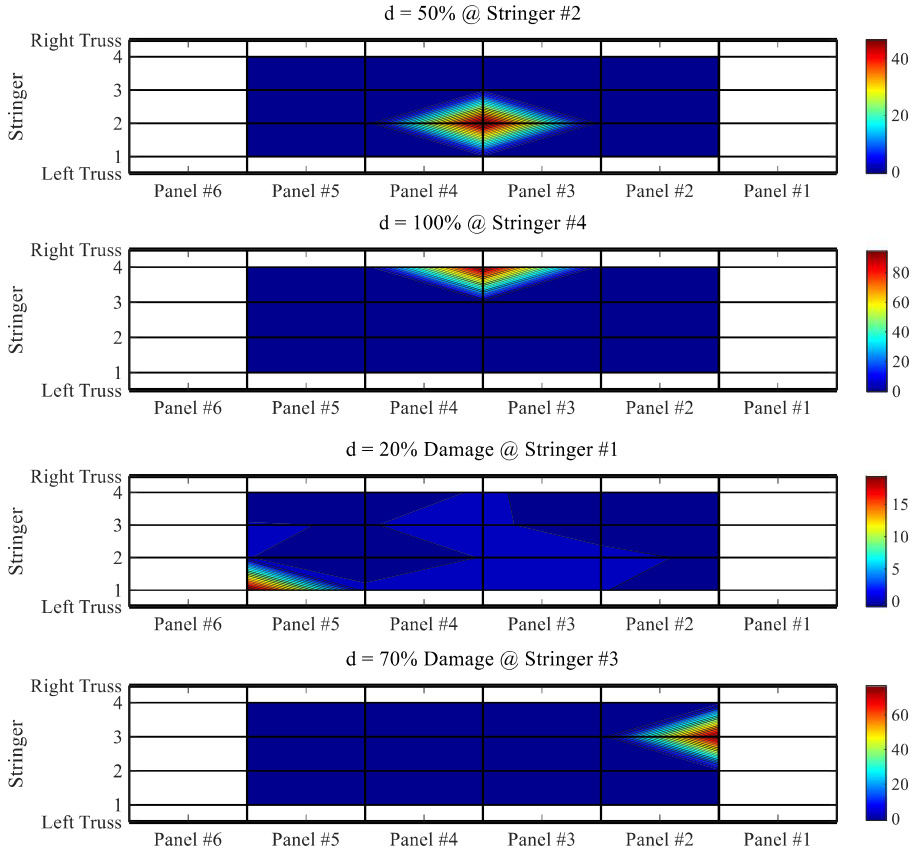

FIGURE 18 Damage contour maps obtained by artificial neural network regression

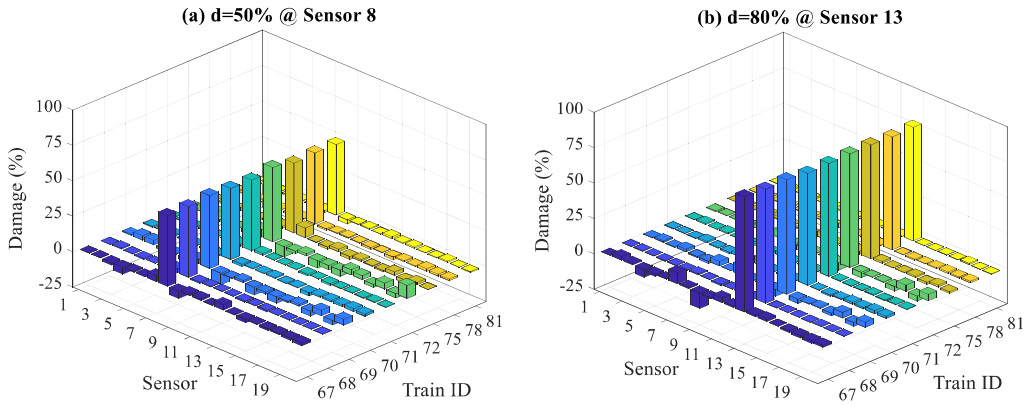

FIGURE 19 Identified damage indexes from artificial neural network regression for (a) d = 50% damage to a connection in vicinity of sensor 8, (a) d = 80% damage to a connection in vicinity of sensor 13: In this case, six train loads were used for artificial neural network training, and the remaining nine train loads were used for artificial neural network validation

A study of the effect of number of loading scenarios on accuracy of damage identification by ANNs was conducted and reported in Figures 19–21. Three cases were considered. In the first case, which was reflected in Figure 19, six Group 4 train loads were randomly picked for ANN training, and the remaining train loads in Group 4 were used for validating ANN damage identification accuracy. In the second and the third case, respectively, eight and nine trains were used for ANN training, and the remaining train loads were used for validation. It was observed that, at the number of loading scenarios in the training ANNs was reduced, the damage identification error increased. The observations confirmed the expectation that, given a sufficient number of train load scenarios, ANNs could be generalized to address future unknown loading scenarios.

To study the effect of categorizing loading scenarios on the damage detection performance of the ANNs trained using Group 4 loads, POMs of bridge responses to the trains in Groups 1, 2, and 3 were also used as inputs to the ANNs. In this case, POMs of the healthy structure were considered to assess the potential of ANNs to generate false positives. In Figure 22, the identified damage indices for the healthy structure are shown, when loading scenarios were selected from Groups 1–4. It was observed that, as the train axle loads become lighter and, therefore, become less relevant to the category of the trains that was used for training the ANN, the error in prediction of damage indices increases. It is noteworthy that none of the train load scenarios used for validation were used for training the ANNs.

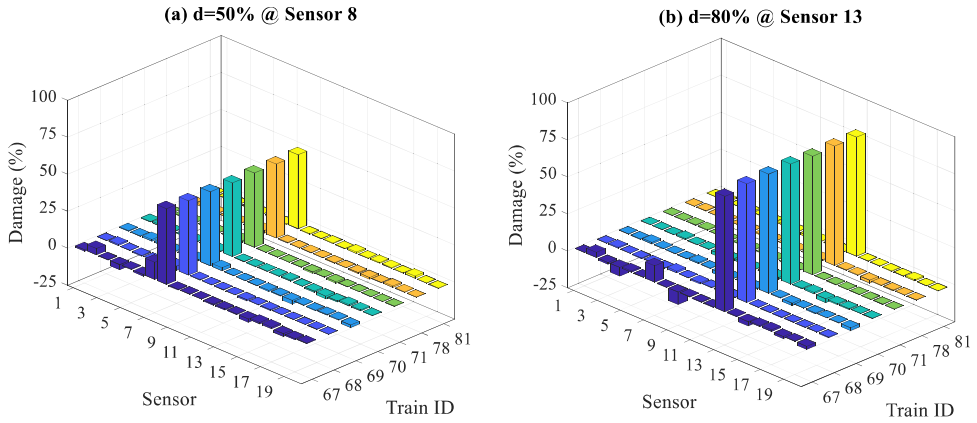

FIGURE 20 Identified damage indexes from artificial neural network regression for (a) d = 50% damage to a connection in vicinity of sensor 8, (a) d = 80% damage to a connection in vicinity of sensor 13: In this case, eight train loads were used for artificial neural network training, and the remaining seven train loads were used for ANN validation

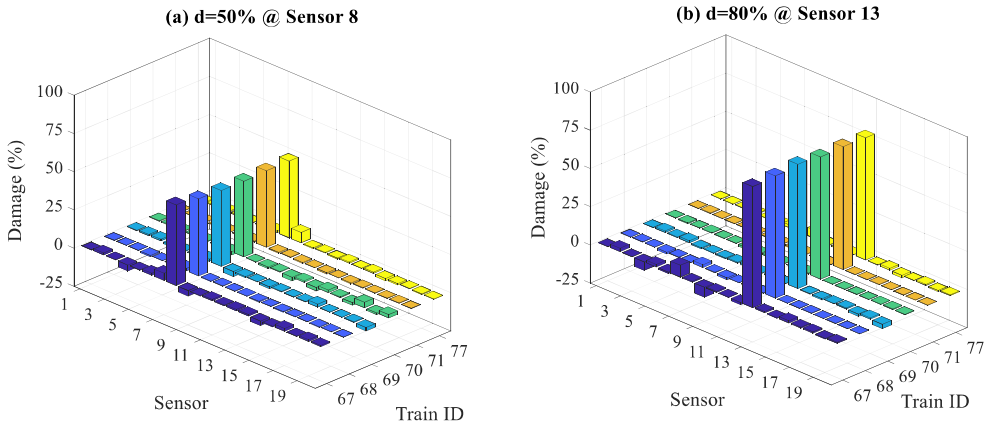

FIGURE 21 Identified damage indexes from artificial neural network regression for (a) d = 50% damage to a connection in vicinity of sensor 8, (a) d = 80% damage to a connection in vicinity of sensor 13: In this case, nine train loads were used for artificial neural network training, and the remaining six train load were used for artificial neural network validation

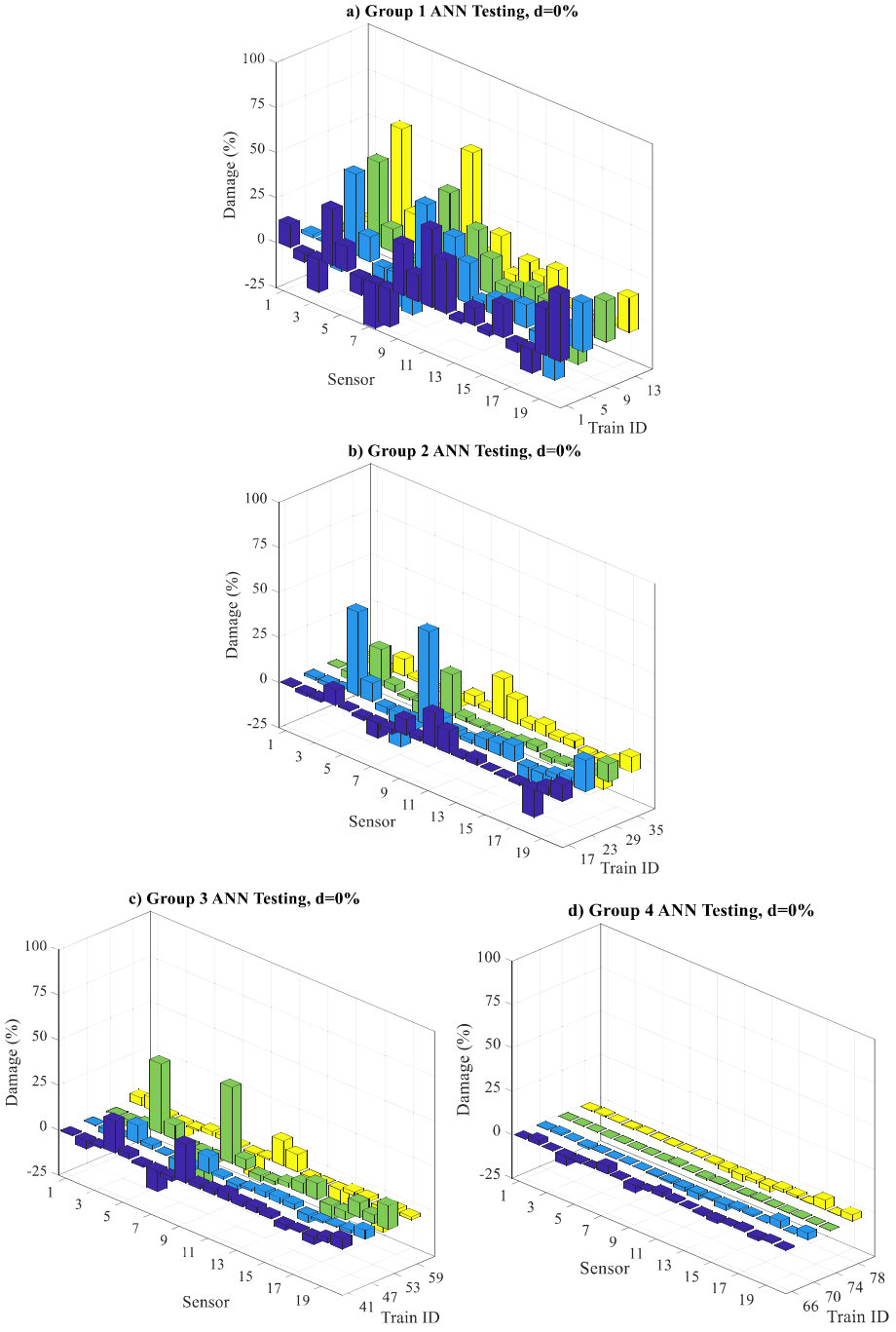

FIGURE 22 Identified damage indexes from artificial neural network regression for no damage (d = 0%) when group 4 trains were used for building the artificial neural network, (a) group 1 loads were used for validation, (b) group 2 loads were used for validation, (c) group 3 loads were used for validation, (d) group 4 loads were used for validation

Finally, to demonstrate ANN performance for identifying lower level damage intensities, the ANN trained using six train load scenarios was validated for lower level intensities. Representative results are shown in Figure 23 for damage intensities equal to 0, 10, 20, and 30% in the vicinity of Sensor 8. Train number 75 was selected for validation; other damage locations and train loads yielded similar results. It was observed that false estimates of damage, approaching 5%, were estimated at undamaged locations by the ANN. Therefore, damage predictions less than 5% were considered erroneous. Should this approach be utilized for continuous monitoring, a statistical analysis of available data would need to be completed to determine probability distributions and help establish erroneous prediction thresholds.

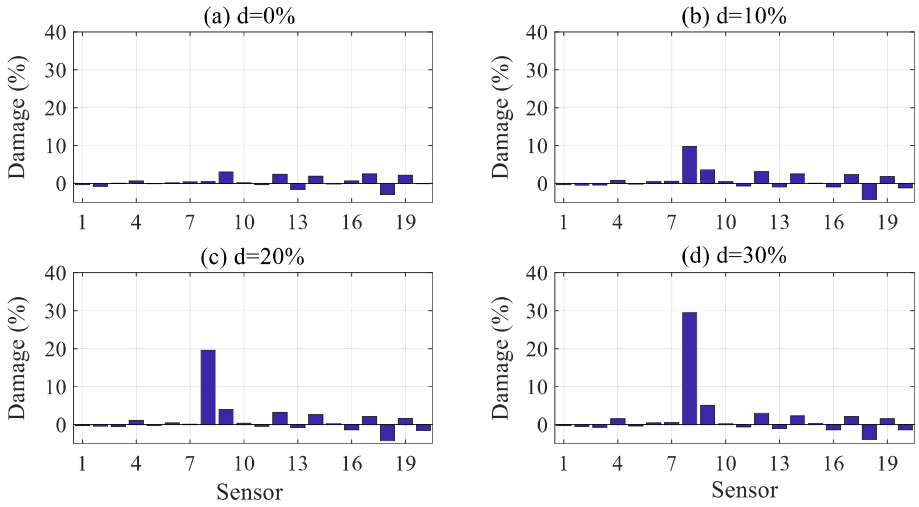

FIGURE 23 Identified damage indexes from artificial neural network regression for connection damage in the vicinity of sensor 8 for (a) d = 0%, (b) d = 10%, (c) d = 20%, and (d) d = 30%: In this case, six train loads were used for artificial neural network training, and the train number 75 load was used for artificial neural network validation

5 | CONCLUSIONS

This paper presents a framework for automated structural damage detection using ANNs and POD. Structural response POMs were adopted as damage features because structures subjected to nonstationary excitations renders POMs dependent on more than damage. The proposed framework was applied to damage detection in a steel railway bridge located in central Nebraska, whose inputs are highly nonstationary for each individual train passage loading scenario. To complete the study, a 3D FE model was constructed for generating pseudoexperimental data, and measured WIM data obtained from the bridge owners was used to supply the inputs. Subsequently, ANNs were used for training a classification and a regression function for categorizing structural response and identifying damage indexes from the categorized response matrixes, namely, snapshot matrixes of each train passage.

It was concluded that

- variations in train speed and train axle load can have marginal effects on POMs; however, relatively small changes could affect damage detection accuracy when other sources for POM variability are present;
- external load location and direction of travel could significantly affect POMs;
- automated peak picking was preferred when selecting data for the snapshot matrix used to calculate POMs;
- categorizing the POMs based on average RMS for all "sensors" could decrease their variability because of train axle loads;
- numerical analysis verified that the regression network can accurately generalize for train load scenarios, which were not used for training the network; and
- the method can effectively identify damage with even relatively low intensities.

ACKNOWLEDGEMENT

The authors also gratefully acknowledge assistance, access, computing resources, data, and expertise provided by the University of Nebraska Lincoln's Holland Computing Center, Union Pacific, and Bridge Diagnostics Inc. in association with this project.

ORCID

Saeed Eftekhar Azam http://orcid.org/0000-0001-8153-5506

REFERENCES

1. Phares BM, Rolander DD, Graybeal BA, Washer GA. *Reliability of Visual Bridge Inspection for Highway Bridges, Volume I: Final Report*. I; 2001.

2. Washer G, Connor R, Nasrollahi M, Provines J. New framework for risk-based inspection of highway bridges. *J Bridg Eng*. 2016;21.
3. Farrar CR, Worden K. *Structural Health Monitoring: A Machine Learning Perspective*. Wiley Publishing; 2012.
4. Shi JY, Spencer BF, Chen SS. Damage detection in shear buildings using different estimated curvature. *Struct Control Health Monit*. 2017.
5. Roy K. Structural damage identification using mode shape slope and curvature. *J Eng Mech*. 2017;143(9).
6. Moaveni B, Conte JP, Hemez FM. Uncertainty and sensitivity analysis of damage identification results obtained using finite element model updating. *Comput Aided Civ Inf Eng*. 2009;24(5):320-334.
7. Moaveni B, He X, Conte JP, Restrepo JI. Damage identification study of a seven-story full-scale building slice tested on the UCSD-NEES shake table. *Struct Saf*. 2010;32(5):347-356.
8. Taciroglu E, Ghahari SF, Abazarsa F. Efficient model updating of a multi-story frame and its foundation stiffness from earthquake records using a timoshenko beam model. *Soil Dyn Earthq Eng*. 2017;92:25-35.
9. Tan ZX, Thambiratnam DP, Chan THT, Abdul Razak H. Detecting damage in steel beams using modal strain energy based damage index and artificial neural network. *Eng Fail Anal*. 2017;79:253-262.
10. Ashory MR, Ghasemi-Ghalebahman A, Kokabi MJ. An efficient modal strain energy-based damage detection for laminated composite plates. *Adv Compos Mater*. 2017;1-16.
11. Moaveni B, Behmanesh I. Effects of changing ambient temperature on finite element model updating of the Dowling hall footbridge. *Eng Struct*. 2012;43:58-68.
12. Hu W-H, Cunha Á, Caetano E, Rohrmann RG, Said S, Teng J. Comparison of different statistical approaches for removing environmental/operational effects for massive data continuously collected from footbridges. *Struct Control Health Monit*. 2017;24(8): e1955-n/a.
13. Ghahari SF, Abazarsa F, Taciroglu E. Blind modal identification of non-classically damped structures under non-stationary excitations. *Struct Control Health Monit*. 2017;24(6).
14. Abazarsa F, Nateghi F, Ghahari SF, Taciroglu E. Extended blind modal identification technique for nonstationary excitations and its verification and validation. *J Eng Mech*. 2016;142:1-19.
15. Moaveni B, He X, Conte JP, Restrepo JI, Panagiotou M. System identification study of a 7-story full-scale building slice tested on the UCSD-NEES shake table. *J Struct Eng*. 2011;137(6):705-717.
16. Moaveni B, Barbosa AR, Conte JP, Hemez FM. Uncertainty analysis of system identification results obtained for a seven-story building slice tested on the UCSD-NEES shake table. *Struct Control Health Monit*. 2014;21(4):466-483.
17. Papadimitriou C, Papadioti D-C. Component mode synthesis techniques for finite element model updating. *Comput Struct*. 2013;126:15-28.
18. Behmanesh I, Moaveni B, Lombaert G, Papadimitriou C. Hierarchical Bayesian model updating for structural identification. *Mech Syst Sig Process*. 2015;64-65:360-376.
19. Behmanesh I, Moaveni B, Papadimitriou C. Probabilistic damage identification of a designed 9-story building using modal data in the presence of modeling errors. *Eng Struct*. 2017;131:542-552.
20. Astroza R, Nguyen LT, Nestorović T. Finite element model updating using simulated annealing hybridized with unscented Kalman filter. *Comput Struct*. 2016;177:176-191.
21. Erazo K, Hernandez EM. A model-based observer for state and stress estimation in structural and mechanical systems: experimental validation. *Mech Syst Sig Process*. 2014;43(1-2):141-152.
22. Astroza R, Ebrahimian H, Li Y, Conte JP. Bayesian nonlinear structural FE model and seismic input identification for damage assessment of civil structures. *Mech Syst Sig Process*. 2017;93:661-687.
23. Eftekhar Azam S, Mariani S, Attari NKA. Online damage detection via a synergy of proper orthogonal decomposition and recursive Bayesian filters. *Nonlinear Dyn*. 2017;1-23.
24. Song W. Generalized minimum variance unbiased joint input-state estimation and its unscented scheme for dynamic systems with direct feedthrough. *Mech Syst Sig Process*. 2018;99:886-920.
25. Worden K, Manson G, Fieller NRJ. Damage detection using outlier analysis. *J Sound Vib*. 2000;229(3):647-667.
26. O'Connor SM, Zhang Y, Lynch JP, Ettouney MM, Jansson PO. Long-term performance assessment of the telegraph road bridge using a permanent wireless monitoring system and automated statistical process control analytics. *Struct Infrastruct Eng*. 2017;13(5):604-624.
27. Dervilis N, Choi M, Taylor SG, et al. On damage diagnosis for a wind turbine blade using pattern recognition. *J Sound Vib*. 2014;333(6):1833-1850.
28. Ou Y, Chatzi EN, Dertimanis VK, Spiridonakos MD. Vibration-based experimental damage detection of a small-scale wind turbine blade. *Struct Health Monit*. 2017;16(1):79-96.
29. Bogoevska S, Spiridonakos M, Chatzi E, Dumova-Jovanoska E, Höffer R. A data-driven diagnostic framework for wind turbine structures: a holistic approach. *Sensors*. 2017;17(4).

30. Yan AM, Kerschen G, De Boe P, Golinval JC. Structural damage diagnosis under varying environmental conditions—part I: a linear analysis. *Mech Syst Sig Process*. 2005;19(4):847-864.

31. Ruotolo R, Surace C. Using svd to detect damage in structures with different operational conditions. *J Sound Vib*. 1999;226(3):425-439.

32. Vanlanduit S, Parloo E, Cauberghe B, Guillaume P, Verboven P. A robust singular value decomposition for damage detection under changing operating conditions and structural uncertainties. *J Sound Vib*. 2005;284(3-5):1033-1050.

33. Galvanetto U, Violaris G. Numerical investigation of a new damage detection method based on proper orthogonal decomposition. *Mech Syst Sig Process*. 2007;21(3):1346-1361.

34. Shane C, Jha R. Proper orthogonal decomposition based algorithm for detecting damage location and severity in composite beams. *Mech Syst Sig Process*. 2011;25(3):1062-1072.

35. Eftekhar Azam S. *Online damage detection in structural systems*. Springer; 2014.

36. Bellino A, Fasana A, Garibaldi L, Marchesiello S. PCA-based detection of damage in time-varying systems. *Mech Syst Sig Process*. 2010;24(7):2250-2260.

37. Lanata F, Del Grosso A. Damage detection and localization for continuous static monitoring of structures using a proper orthogonal decomposition of signals. *Smart Mater Struct*. 2006;15(6):1811-1829.

38. Xia Q, Tian YD, Zhu XW, Xu DW, Zhang J. Structural damage detection by principle component analysis of long-gauge dynamic strains. *Struct Eng Mech*. 2015;54(2):379-392.

39. Eftekhar Azam S, Mariani S. Investigation of computational and accuracy issues in POD-based reduced order modeling of dynamic structural systems. *Eng Struct*. 2013;54:150-167.

40. Zang C, Friswell MI, Imregun M. Structural damage detection using independent component analysis. *Structural Health Monitoring*. 2004;3(1):69-83.

41. Jin C, Jang S, Sun X, Li J, Christenson R. Damage detection of a highway bridge under severe temperature changes using extended Kalman filter trained neural network. *J Civ Struct Heal Monit*. 2016;6(3):545-560.

42. Dworakowski Z, Dragan K, Stepinski T. Artificial neural network ensembles for fatigue damage detection in aircraft. *J Intell Mater Syst Struct*. 2017;28(7):851-861.

43. Gu J, Gul M, Wu X. Damage detection under varying temperature using artificial neural networks. *Struct Control Health Monit*. 2017;24(11):e1998.

44. Sbarufatti C. Optimization of an artificial neural network for fatigue damage identification using analysis of variance. *Struct Control Health Monit*. 2017;24(9):e1964.

45. Amezquita-Sanchez JP, Adeli H. Feature extraction and classification techniques for health monitoring of structures. *Sci Iran*. 2015;22:1931-1940.

46. Buljak V. *Inverse analyses with model reduction: proper orthogonal decomposition in structural mechanics*. Springer Science & Business Media; 2011.

47. Pearson K. On lines and planes of closest fit to systems of points in space. *Philos Mag*. 1901;2:559-572.

48. Karhunen K. *Uber lineare methoden in der wahrscheinlichkeitsrechnung*. *Annales Academiae Scientiarum Fennicae, Series A1: Mathematica-Physica*. 37; 1947:3-79.

49. Klema VC, Laub AJ. The singular value decomposition: its computation and some applications. *IEEE Trans Autom Control*. 1980;25(2):164-176.

50. Liang YC, Lee HP, Lim SP, Lin WZ, Lee KH, Wu CG. Proper orthogonal decomposition and its applications—part I: theory. *J Sound Vib*. 2002;252(3):527-544.

51. Hyvärinen A. Independent component analysis: recent advances. *Philos Trans R Soc A Math Phys Eng Sci*. 371:2013.

52. Poncelet F, Kerschen G, Golinval J-C, Verhelst D. Output-only modal analysis using blind source separation techniques. *Mech Syst Sig Process*. 2007;21(6):2335-2358.

53. Yang Y, Nagarajaiah S. Time-frequency blind source separation using independent component analysis for output-only modal identification of highly damped structures. *J Struct Eng*. 2012;139:1780-1793.

54. Feeny B, Kappagantu R. On the physical interpretation of proper orthogonal modes in vibrations. *J Sound Vib*. 1998;211(4):607-616.

55. Kerschen G, Golinval GC. Physical interpretation of the proper orthogonal modes using the singular value decomposition. *J Sound Vib*. 2002;249(5):849-865.

56. Feeny B. On proper orthogonal co-ordinates as indicators of modal activity. *J Sound Vib*. 2002;255(5):805-817.

57. Georgiou I. Advanced proper orthogonal decomposition tools: using reduced order models to identify normal modes of vibration and slow invariant manifolds in the dynamics of planar nonlinear rods. *Nonlinear Dyn*. 2005;41(1-3):69-110.

58. Yadalam VK, Feeny B. Reduced mass-weighted proper decomposition for modal analysis. *J Vib Acoust*. 2011;133(2):024504.

59. Kerschen G, Golinval J-c, Vakakis AF, Bergman LA. The method of proper orthogonal decomposition for dynamical characterization and order reduction of mechanical systems: an overview. *Nonlinear Dyn*. 2005;41(1-3):147-169.
60. North GR. Empirical orthogonal functions and normal modes. *J Atmos Sci*. 1984;41(5):879-887.
61. Schilders WH. Introduction to model order reduction. In: Schilders WH, Van der Vorst HA, Rommes J, eds. *Model Order Reduction. Theory, Research Aspects and Applications*. 1st ed. Springer; 2008.
62. Demuth H, Beale M, Hagan M. *Neural Tetwork Toolbox For Use with MATLAB*. The MathWorks Inc.; 2000.
63. Bishop CM. *Pattern recognition and machine learning*. springer; 2006.
64. MacKay DJ. Bayesian interpolation. *Neural Comput*. 1992;4(3):415-447.
65. Nguyen D, Widrow B. Improving the learning speed of 2-layer neural networks by choosing initial values of the adaptive weights. In: 1990 *IJCNN International Joint Conference on Neural Networks*, 1990; 21–26.
66. Waszczyszyn Z. Fundamentals of Artificial Neural Networks. In: Waszczyszyn Z, ed. *Neural Networks in the Analysis and Design of Structures*. Vienna: Springer Vienna; 1999:1-51.
67. Foresee FD, Hagan MT. Gauss-Newton Approximation to Bayesian Learning. In: *Neural networks, 1997, international conference on*, 1997; 1930–1935.
68. Wilson E, Habibullah A. SAP2000 Integrated Finite Element Analysis and Design of Structures Basic Analysis Refence Manual. 1998.
69. Rageh A. *Optimized Health Monitoring Plans for a Steel, Double-Track Railway Bridge*. Lincoln, NE, USA: Masters, Department of Civil Engineering, University of Nebraska–Lincoln; 2018.
70. Moler C. *MATLAB User's Guide vol. 5*. The Mathworks: Natick, MA, United States; 1998.
71. Fawcett T. An introduction to ROC analysis. *Pattern Recogn Lett*. 2006;27(8):861-874.
72. Simoen E, Papadimitriou C, Lombaert G. On prediction error correlation in Bayesian model updating. *J Sound Vib*. 2013;332(18):4136-4152.
73. Al-Emrani M. Fatigue performance of stringer-to-floor-beam connections in riveted railway bridges. *J Bridg Eng*. 2005;10(2):179-185.
74. Haghani R, Al-Emrani M, Heshmati M. Fatigue-prone details in steel bridges. *Buildings*. 2012;2(4):456-476.

How to cite this article: Eftekhar Azam S, Rageh A, Linzell D. Damage detection in structural systems utilizing artificial neural networks and proper orthogonal decomposition. *Struct Control Health Monit*. 2018;e2288. https://doi.org/10.1002/stc.2288

APPENDIX

BRIDGE DESCRIPTION

Each truss span consists of two main trusses with train rails resting on ties supported by longitudinal stringers. These stringers frame into transverse floor beams spanning between truss lower chord panel points. Lateral bracing existed between the stringers and truss lower chords, with the truss top chord being braced using a combination of lateral bracing and transverse struts. A summary of the types of structural elements used for the truss and floor system, along with relevant cross sectional information, can be found in Table A1.

The most common deficiencies reported in the literature for this type of bridge are development of fatigue cracks at clip-angle, connections between the stringers, and floor beams.[74] Development of fatigue cracks in stringer to floor beam clip angles was simulated by reducing connection rotational stiffness. It was assumed that the moment–rotation relationship at the connection was linear for both healthy and damaged cases, with a healthy connection featuring a rotational stiffness equal to 67% of a continuous stringer span.[73] An isometric view of the FE model is shown in Figure 3.

TABLE A1 Truss structural members and dimensions

Structural member	Description	Dimensions (cm)
Bottom chord	Members (L0–L2) and (L4–L6) riveted built-up sections Members (L2–L4) eyebars	61.0 D × 66.0 W 20.3 D × 5.1 T
Top chord	Riveted built-up sections	61.0 D × 76.2 W
Verticals	Diagonal (L0–U1) riveted built-up section Vertical (L1–U1) riveted built-up section Interior verticals riveted built-up section	39.4 D × 47.5 W 43.2 D × 42.2 W 61.0 D × 76.2 W
Diagonals	Eyebars	15.2 W × 2.5 T; 17.8 W × 4.1 T; 17.8 W × 4.8 T; 20.3 W × 5.1 T
Stringers	Riveted built-up I-section	121.9 D × 31.5 W
Floor beams	Exterior riveted built-up I-section Interior riveted built-up I-section	161.3 D × 35.6 W 164.6 D × 35.6 W
Bottom laterals	Single angles	15.2 × 10.8 × 1.3 15.2 × 10.8 × 1.0
Stringer laterals	Single angles	7.6 × 7.6 × 1.0
Truss top portals	End portal (U1 and U5) Interior portals (U2, U3, and U4)	182.9 D, chords 2 angles 15.2 × 10.8 × 1.3 Diagonals single angles 8.9 × 7.6 × 1 30.5 D, chords 2 angles 15.2 × 8.9 × 1 diagonals laced plates 6.4 × 1
Truss upper lateral bracing	The lateral bracing members in between top portals	30.5 D Chords single angle 8.9 × 8.9 × 1 Diagonals laced plates 6.4 × 1

Note. D: depth, T: thickness, W: width.